

Preparing highly entangled states of nanodiamond rotation and NV center spin

Wen-Liang Li(李文亮) and Duan-Lu Zhou(周端陆)
Citation: Chin. Phys. B, 2024, 33 (**2**): 020305. DOI: 10.1088/1674-1056/ad117a
Journal homepage: http://cpb.iphy.ac.cn; http://iopscience.iop.org/cpb

What follows is a list of articles you may be interested in

Sharing quantum nonlocality in the noisy scenario

Shu-Yuan Yang(杨舒媛), Jin-Chuan Hou(侯晋川), and Kan He(贺衍)
Chin. Phys. B, 2024, 33 (**1**): 010302. DOI: 10.1088/1674-1056/ad062d

Generation of hyperentangled photon pairs based on lithium niobate waveguide

Yang-He Chen(陈洋河), Zhen Jiang(姜震), and Guang-Qiang He(何广强)
Chin. Phys. B, 2023, 32 (**9**): 090306. DOI: 10.1088/1674-1056/acd5c4

Commensurate and incommensurate Haldane phases for a spin-1 bilinear-biquadratic model

Yan-Wei Dai(代艳伟), Ai-Min Chen(陈爱民), Xi-Jing Liu(刘希婧), and Yao-Heng Su(苏耀恒)
Chin. Phys. B, 2023, 32 (**9**): 090304. DOI: 10.1088/1674-1056/acac0c

Orientation determination of nitrogen-vacancy center in diamond using a static magnetic field

Yangpeng Wang(王杨鹏), Rujian Zhang(章如健), Yan Yang(杨燕), Qin Wu(吴琴), Zhifei Yu(于志飞), and Bing Chen(陈冰)
Chin. Phys. B, 2023, 32 (**7**): 070301. DOI: 10.1088/1674-1056/acc0f7

Heralded entanglement purification protocol using high-fidelity parity-check gate based on nitrogen-vacancy center in optical cavity

Lu-Cong Lu(陆路聪), Guan-Yu Wang(王冠玉), Bao-Cang Ren(任宝藏), Mei Zhang(章梅), Fu-Guo Deng(邓富国)
Chin. Phys. B, 2020, 29 (**1**): 010305. DOI: 10.1088/1674-1056/ab5939

Preparing highly entangled states of nanodiamond rotation and NV center spin

Wen-Liang Li(李文亮)[1,2] and Duan-Lu Zhou(周端陆)[1,2,†]

[1] *Institute of Physics, Beijing National Laboratory for Condensed Matter Physics, Chinese Academy of Sciences, Beijing* 100190, *China*
[2] *School of Physical Sciences, University of Chinese Academy of Sciences, Beijing* 100049, *China*

(Received 12 October 2023; revised manuscript received 27 November 2023; accepted manuscript online 1 December 2023)

A nanodiamond with an embedded nitrogen-vacancy (NV) center is one of the experimental systems that can be coherently manipulated within current technologies. Entanglement between NV center electron spin and mechanical rotation of the nanodiamond plays a fundamental role in building a quantum network connecting these microscopic and mesoscopic degrees of motions. Here we present a protocol to asymptotically prepare a highly entangled state of the total quantum angular momentum and electron spin by adiabatically boosting the external magnetic field.

Keywords: nanodiamond, NV center, entanglement

PACS: 03.65.–w, 03.65.Ud, 03.65.Aa **DOI:** 10.1088/1674-1056/ad117a

1. Introduction

Experimental accomplishments of cooling and controlling of micro-nano scale particles make it possible to exploit macroscopic quantum systems. The nitrogen-vacancy (NV) centers in diamond have shown impressive applications in quantum sensing, quantum information processing and communications.[1–3] Nanodiamonds with NV centers trapped in vacuum can be cooled into their center-of-mass ground state[4–6] and be used to generate spatial quantum superpositions.[7–10] While in recent years the rotation control of nanoparticle with ultra-high precision[11–15] opens the path to observing and testing rotational superpositions.[16–21] In view of quantum information, the coupling of NV center spin and the nanodiamond rotation contains entanglement resource.[22] Study of the entanglement property of the spin–rotation coupled system may have potential use in quantum sensing and quantum network.

In this paper, we simplify the system to an ideal model by considering the nanodiamond only in an external magnetic field. The nanodiamond is treated as a rigid body and its rotation can be described by angular momentum theory in quantum physics.[23–25] We show that by boosting the external magnetic field strength, a highly entangled state of NV center spin and total angular momentum can be realized asymptotically.

2. Our model and problem

As shown in Fig. 2, we consider a nanodiamond, modeled as a symmetric top whose shape is a tetrahedron. The nanodiamond hosts a single negatively charged nitrogen-vacancy center (NV^-) with the spin angular momentum $\hat{\boldsymbol{S}}$ whose quantization axis is aligned with the nanodiamond symmetric axis. The ground state structure of the spin-1 NV^- center is shown in Fig. 1. We suppose the nanodiamond's mechanic rotation is free. In a magnetic field $\boldsymbol{B} = B\boldsymbol{e}_3$ along the $\boldsymbol{e}_3$-direction of the space-fixed frame with axes $\{\boldsymbol{e}_1, \boldsymbol{e}_2, \boldsymbol{e}_3\}$, the spin of the NV^- center and the rotation of the diamond are coupled, and the system is described by the Hamiltonian

$$H = H_0 + V, \tag{1}$$

with

$$H_0 = \hbar D\hat{S}_3'^2 + \frac{\hbar^2}{2}\frac{\hat{\boldsymbol{L}}^2}{I_1} + \frac{\hbar^2}{2}\left(\frac{1}{I_3} - \frac{1}{I_1}\right)\hat{L}_3'^2, \tag{2}$$

$$V = g\mu_{\rm B}B\sum_{i=1}^{3}\hat{S}_i'\hat{\boldsymbol{e}}_i'\cdot\boldsymbol{e}_3, \tag{3}$$

where $\{\hat{\boldsymbol{e}}_1', \hat{\boldsymbol{e}}_2', \hat{\boldsymbol{e}}_3'\}$ are the principle axes of the nanodiamond and form the body-fixed frame, which are dynamic operators related with rotations. $\hbar\hat{\boldsymbol{L}}$ is the rotation angular momentum operator. $\{I_1, I_2, I_3\}$ are the principle inertia moments with $I_1 = I_2$ for a symmetric top. $\hat{S}_i'$ ($\hat{L}_i'$) is the projection component operator of $\hat{\boldsymbol{S}}$ ($\hat{\boldsymbol{L}}$) along the body-fixed $\boldsymbol{e}_i'$-axis. $\mu_{\rm B}$ is the Bohr magneton. The zero-field-splitting of the spin triplet ground state $D \simeq (2\pi)2.87$ GHz, and the isotropic NV^- center electron g-factor $g \simeq 2.0028$.[26]

When we write the Hamiltonian in body frame, we should be careful about the commutation relations of the operators especially in different coordinate frames.[27] Notice that the spin components $\hat{S}_i'$ are not commuting with the angular momentum components $\hat{L}_i$ since $\hat{S}_i' \equiv \hat{\boldsymbol{e}}_i'\cdot\hat{\boldsymbol{S}}$, we introduce the total angular momentum operator $\hat{\boldsymbol{J}} = \hat{\boldsymbol{L}} + \hat{\boldsymbol{S}}$ which gives commutation relations $[\hat{J}_i', \hat{S}_j'] = 0$ and $[\hat{J}_3, \hat{S}_3'] = 0$.

†Corresponding author. E-mail: zhoudl72@iphy.ac.cn

© 2024 Chinese Physical Society and IOP Publishing Ltd

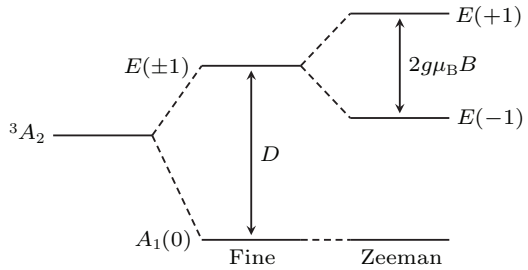


Fig. 1. The fine and Zeeman structures of the NV$^-$ center ground state. The structure levels are denoted by their spin–orbit symmetry and spin projections $m \in \{0, \pm 1\}$.

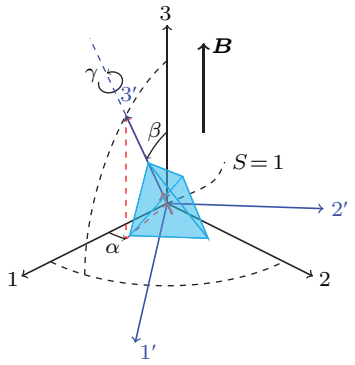


Fig. 2. Sketch of the nanodiamond with an embedded NV$^-$ center in external magnetic field B. $\{\alpha, \beta, \gamma\}$ are Euler angles between the space-fixed frame and the body-fixed frame.

The problem we aim to solve is how the entanglement between nanodiamond's total angular momentum and its spin in the thermal equilibrium state varies as a function of magnetic field and temperature, where the thermal state is

$$\rho(B,T) = \frac{\mathrm{e}^{-\beta H}}{\mathrm{Tr}\,\mathrm{e}^{-\beta H}}, \tag{4}$$

where $\beta = \frac{1}{k_\mathrm{B} T}$ with k_B being the Boltzmann constant. As the temperature approaches to zero, the thermal equilibrium state becomes the ground state

$$\lim_{T\to 0} \rho(B,T) = |G(B)\rangle\langle G(B)|. \tag{5}$$

3. Eigen problem of the Hamiltonian

Before exploring the entanglement between the total angular momentum and the spin in the thermal equilibrium state $\rho(B,T)$ or in the ground state $|G(B)\rangle$, it is necessary for us to solve the eigen problem of the Hamiltonian (1). Rewrite the Hamiltonian by inserting $\hat{\boldsymbol{L}} = \hat{\boldsymbol{J}} - \hat{\boldsymbol{S}} = \hat{\boldsymbol{J}} + \hat{\boldsymbol{K}}$,

$$\begin{aligned} H_0 &= \hbar D \hat{K}_3'^2 + \frac{\hbar^2}{2I_1}(\hat{\boldsymbol{J}}^2 + 2\hat{J}_3'\hat{K}_3' + \hat{J}_+'\hat{K}_-' + \hat{J}_-'\hat{K}_+') \\ &\quad + \hbar^2\left(\frac{1}{I_3} - \frac{1}{I_1}\right)\frac{(\hat{J}_3' + \hat{K}_3')^2}{2}, \\ V &= -g\mu_\mathrm{B}\hat{\boldsymbol{K}}\cdot\boldsymbol{B}, \end{aligned} \tag{6}$$

where we have let $\hat{\boldsymbol{K}} \equiv -\hat{\boldsymbol{S}}$ with $K \equiv S \equiv 1$ in our problem and dropped $\hat{\boldsymbol{S}}^2 = S(S+1)$. And the ladder operators are

$$\hat{J}_\pm' = \hat{J}_1' \mp \mathrm{i}\hat{J}_2', \quad \hat{K}_\pm' = \hat{K}_1' \mp \mathrm{i}\hat{K}_2'. \tag{7}$$

3.1. Basis states based on H_0

First we study the degree of the nanodiamond rotation. Because $\hat{\boldsymbol{L}}$ is an angular momentum operator, it obeys the following commutation relations:

$$[\hat{L}_i, \hat{L}_j] = \mathrm{i}\sum_k \varepsilon_{ijk}\hat{L}_k, \quad [\hat{L}_i, \hat{\boldsymbol{e}}_l'\cdot\boldsymbol{e}_j] = \mathrm{i}\sum_k \varepsilon_{ijk}\hat{\boldsymbol{e}}_l'\cdot\boldsymbol{e}_k, \tag{8}$$

where $i,j,k \in \{1,2,3\}$ and $l \in \{1,2,3\}$, and ε_{ijk} is antisymmetric tensor with $\varepsilon_{123} = 1$. Note that $\hat{L}_i' \equiv \hat{\boldsymbol{e}}_i'\cdot\hat{\boldsymbol{L}}$. Then a direct calculation gives

$$[\hat{L}_i', \hat{L}_j'] = -\mathrm{i}\sum_k \varepsilon_{ijk}\hat{L}_k', \tag{9}$$

where $i,j,k \in \{1,2,3\}$. Comparing Eq. (9) with Eq. (8), it is interesting to observe that a negative sign appears in the commutation relations of the angular momentum in the body-fixed frame. With the relations $\hat{S}_i' \equiv \hat{\boldsymbol{e}}_i'\cdot\hat{\boldsymbol{S}} = \sum_{j=1}^3 \hat{\boldsymbol{e}}_i'\cdot\boldsymbol{e}_j\hat{S}_j$, one can obtain the following commutation relations:

$$[\hat{J}_i', \hat{J}_j'] = -\mathrm{i}\sum_k \varepsilon_{ijk}\hat{J}_k', \quad [\hat{K}_i', \hat{K}_j'] = -\mathrm{i}\sum_k \varepsilon_{ijk}\hat{K}_k', \tag{10}$$

$$[\hat{J}_i', \hat{K}_j'] = 0, \quad [\hat{J}_i, \hat{K}_j'] = 0. \tag{11}$$

The total angular momentum $\hat{\boldsymbol{J}}^2 = \sum_i \hat{J}_i^2 = \sum_i \hat{J}_i'^2$, which builds a relation between the angular momentum operators in these two frames. Then we find that

$$[\hat{\boldsymbol{J}}^2, \hat{J}_3] = 0, \quad [\hat{\boldsymbol{J}}^2, \hat{J}_3'] = 0, \quad [\hat{J}_3, \hat{J}_3'] = 0, \tag{12}$$

which implies that $\{\hat{\boldsymbol{J}}^2, \hat{J}_3, \hat{J}_3', \hat{\boldsymbol{K}}^2, \hat{K}_3'\}$ forms a complete set of commuting observables for the degree of freedom of the system. They have the common eigenstates

$$|\varphi\rangle = |Jm_J k_J, Kk_K\rangle, \tag{13}$$

such that

$$\hat{\boldsymbol{J}}^2|\varphi\rangle = J(J+1)|\varphi\rangle, \tag{14}$$

$$\hat{J}_3|\varphi\rangle = m_J|\varphi\rangle, \tag{15}$$

$$\hat{J}_3'|\varphi\rangle = k_J|\varphi\rangle, \tag{16}$$

$$\hat{\boldsymbol{K}}^2|\varphi\rangle = K(K+1)|\varphi\rangle, \tag{17}$$

$$\hat{K}_3'|\varphi\rangle = k_K|\varphi\rangle, \tag{18}$$

where $J \in \{0,1,\ldots\}$, $m_J, k_J \in \{-J, -J+1, \ldots, J-1, J\}$, $k_K \in \{-1,0,1\}$. And these common eigenstates form a set of base vectors of the full Hilbert space. Then the matrix elements of the ladder operators $\hat{J}_\pm'$ and $\hat{K}_\pm'$ are given by the following relations:

$$\begin{aligned} &\hat{J}_\pm'|Jm_J k_J, Kk_K\rangle \\ &= \sqrt{(J\mp k_J)(J\pm k_J+1)}|Jm_J k_J \pm 1, Kk_K\rangle, \end{aligned} \tag{19}$$

$$\begin{aligned} &\hat{K}_\pm'|Jm_J k_J, Kk_K\rangle \\ &= \sqrt{(K\mp k_K)(K\pm k_K+1)}|Jm_J k_J, Kk_K \pm 1\rangle. \end{aligned} \tag{20}$$

For $K=1$, it is convenient to write out the $\hat{K}'_i$ matrices

$$K'_1=\frac{1}{\sqrt{2}}\begin{pmatrix}0&1&0\\1&0&1\\0&1&0\end{pmatrix}, \tag{21}$$

$$K'_2=\frac{-\mathrm{i}}{\sqrt{2}}\begin{pmatrix}0&-1&0\\1&0&-1\\0&1&0\end{pmatrix}, \tag{22}$$

$$K'_3=\begin{pmatrix}1&0&0\\0&0&0\\0&0&-1\end{pmatrix}. \tag{23}$$

3.2. Analytical matrix elements in V

The next task is to calculate the matrix element $\langle J'm'_Jk'_J,Kk'_K|V|Jm_Jk_J,Kk_K\rangle$. In other words, we need to calculate the matrix elements $\langle J'm'_Jk'_J|\hat{e}'_i\cdot e_j|Jm_Jk_J\rangle$.

Because all the operators $\{\hat{e}'_l\cdot e_i\}$ are commutative to each other, we can introduce their common eigenstates

$$\hat{e}'_l\cdot e_i|\alpha\beta\gamma\rangle=e'_l\cdot e_i|\alpha\beta\gamma\rangle, \tag{24}$$

where $\{\alpha,\beta,\gamma\}$ are three Euler angles (illustrated in Fig. 2). In particular

$$\hat{e}'_1\cdot e_3|\alpha\beta\gamma\rangle=-\cos\gamma\sin\beta|\alpha\beta\gamma\rangle, \tag{25}$$

$$\hat{e}'_2\cdot e_3|\alpha\beta\gamma\rangle=\sin\gamma\sin\beta|\alpha\beta\gamma\rangle, \tag{26}$$

$$\hat{e}'_3\cdot e_3|\alpha\beta\gamma\rangle=\cos\beta|\alpha\beta\gamma\rangle. \tag{27}$$

Then

$$\begin{aligned}&\langle J'm'_Jk'_J|\hat{e}'_i\cdot e_3|Jm_Jk_J\rangle\\&=\int \mathrm{d}\omega e'_i\cdot e_3\langle J'm'_Jk'_J|\alpha\beta\gamma\rangle\langle\alpha\beta\gamma|Jm_Jk_J\rangle,\end{aligned} \tag{28}$$

where $\mathrm{d}\omega=\sin\beta\mathrm{d}\alpha\mathrm{d}\beta\mathrm{d}\gamma$ with $\alpha,\gamma\in[0,2\pi]$ and $\beta\in[0,\pi]$. The eigenfunction $\langle\alpha\beta\gamma|Jm_Jk_J\rangle$ can be written as

$$\langle\alpha\beta\gamma|Jm_Jk_J\rangle=\sqrt{\frac{2J+1}{8\pi^2}}D^{(J)}_{k_Jm_J}(\alpha,\beta,\gamma), \tag{29}$$

where $D^{(J)}_{k_Jm_J}(\alpha,\beta,\gamma)$ is the matrix representation of Euler rotation operator $\hat{R}(\alpha,\beta,\gamma)$ in Hilbert space (more details see Appendix A). The D-matrix in this paper takes the definition from Landau's textbook[24] which is the Hermitian conjugate of the Wigner-D matrix conventionally used.

A set of spherical basis vectors in the space-fixed frame can be defined as

$$\xi_{+1}\equiv-(e_1+\mathrm{i}e_2)/\sqrt{2}, \tag{30}$$

$$\xi_0\equiv e_3, \tag{31}$$

$$\xi_{-1}\equiv(e_1-\mathrm{i}e_2)/\sqrt{2}, \tag{32}$$

with the orthogonality relations $\xi^*_\mu\cdot\xi_\nu=\delta_{\mu\nu}$, where $\nu,\mu\in\{+1,0,-1\}$, and ξ^*_μ is the complex conjugate of ξ_μ. Then we can show that $\{\xi_\mu\}$ and $\{\xi'_\mu\}$ obey the transformation

$$\xi_\mu=\sum_\nu D^{(1)}_{\nu\mu}(\alpha,\beta,\gamma)\xi'_\nu. \tag{33}$$

Combining Eqs. (30)–(33), we have

$$\xi'^*_\mu\cdot e_3=\xi'^*_\mu\cdot\xi_0=D^{(1)}_{\mu0}(\alpha,\beta,\gamma). \tag{34}$$

Then

$$\begin{aligned}e'_1\cdot e_3&=\left(-D^{(1)}_{10}(\alpha,\beta,\gamma)+D^{(1)}_{-1\,0}(\alpha,\beta,\gamma)\right)/\sqrt{2},\\e'_2\cdot e_3&=-\mathrm{i}\left(D^{(1)}_{10}(\alpha,\beta,\gamma)+D^{(1)}_{-1\,0}(\alpha,\beta,\gamma)\right)/\sqrt{2},\\e'_3\cdot e_3&=D^{(1)}_{00}(\alpha,\beta,\gamma).\end{aligned} \tag{35}$$

Employing the identity of the integral of three $D^{(J)}_{\nu\mu}(\alpha,\beta,\gamma)$ functions

$$\begin{aligned}&\int D^{(J_1)}_{m'_1m_1}(\alpha,\beta,\gamma)D^{(J_2)}_{m'_2m_2}(\alpha,\beta,\gamma)D^{(J_3)}_{m'_3m_3}(\alpha,\beta,\gamma)\frac{\mathrm{d}\omega}{8\pi^2}\\&=\begin{pmatrix}J_1&J_2&J_3\\m'_1&m'_2&m'_3\end{pmatrix}\begin{pmatrix}J_1&J_2&J_3\\m_1&m_2&m_3\end{pmatrix},\end{aligned} \tag{36}$$

and their complex conjugate relations

$$D^{(J)*}_{\nu\mu}(\alpha,\beta,\gamma)=(-1)^{\nu-\mu}D^{(J)}_{-\nu,-\mu}(\alpha,\beta,\gamma), \tag{37}$$

we arrive at an analytical result of the integral

$$\begin{aligned}&\langle J'm'_Jk'_J|D^{(1)}_{\mu0}(\alpha,\beta,\gamma)|Jm_Jk_J\rangle\\&=\int\frac{\mathrm{d}\omega}{8\pi^2}\sqrt{(2J'+1)(2J+1)}\\&\quad\times D^{(J')*}_{k'_Jm'_J}(\alpha,\beta,\gamma)D^{(1)}_{\mu0}(\alpha,\beta,\gamma)D^{(J)}_{k_Jm_J}(\alpha,\beta,\gamma)\\&=(-1)^{k'_J-m'_J}\sqrt{(2J'+1)(2J+1)}\\&\quad\times\begin{pmatrix}J'&1&J\\-k'_J&\mu&k_J\end{pmatrix}\begin{pmatrix}J'&1&J\\-m'_J&0&m_J\end{pmatrix},\end{aligned} \tag{38}$$

where the right hand side of Eq. (36) is two $3J$-symbols. Inserting Eqs. (38) and (35) into Eq. (28), we get the matrix element $\langle J'm'_Jk'_J|\hat{e}'_i\cdot e_3|Jm_Jk_J\rangle$. Together with $\hat{K}'_i$, we get the matrix element $\langle J'm'_Jk'_J,Kk'_K|V|Jm_Jk_J,Kk_K\rangle$.

3.3. Numerical results on eigen energies

Before numerical solving the eigen problem of Hamiltonian H, we first need to give the values of the inertia momentum $\{I_1,I_2,I_3\}$, which are determined by the nanodiamond size. Extremely small (2–5 nm) nanodiamond with an embedded NV center has been reported in recent experiment.[28] In our calculations, we take the bottom side length of the nanodiamond $a=1$ nm and height $h=1.225$ nm, which leads to $I_1=5.06\times10^{-44}\ \mathrm{kg\cdot m^2}$ and $I_3=3.11\times10^{-44}\ \mathrm{kg\cdot m^2}$.

Since we focus on low energy physics of our system, it is natural to introduce a cutoff via a maximum angular momentum $J_{\max}$ in our numerical calculations. To ensure the convergence of our physical results, we set $J_{\max}=4$ (convergence tests see Appendix B). Then we solve the eigen equation of full Hamiltonian

$$H|\Psi_i\rangle=E_i|\Psi_i\rangle, \tag{39}$$

where

$$|\Psi_i\rangle = \sum_{Jm_Jk_Jk_K}^{J\leq J_{\max}} c^{(i)}_{Jm_Jk_Jk_K} |Jm_J k_J, Kk_K\rangle. \tag{40}$$

The energy levels are shown in Fig. 3(b). As a comparison, Fig. 3(a) shows the energy levels of the effective spin Hamiltonian

$$H_S = \hbar D\hat{S}_3^2 + g\mu_B B\hat{S}_3, \tag{41}$$

which generally describes a resting NV^- center with magnetic field $\boldsymbol{B} = B\boldsymbol{e}_3$ in NV^- axis. While, in our rotating nanodiamond model the direction of NV^- axis is given by the quantum state of angular momentum and not along the direction of the fixed magnetic field.

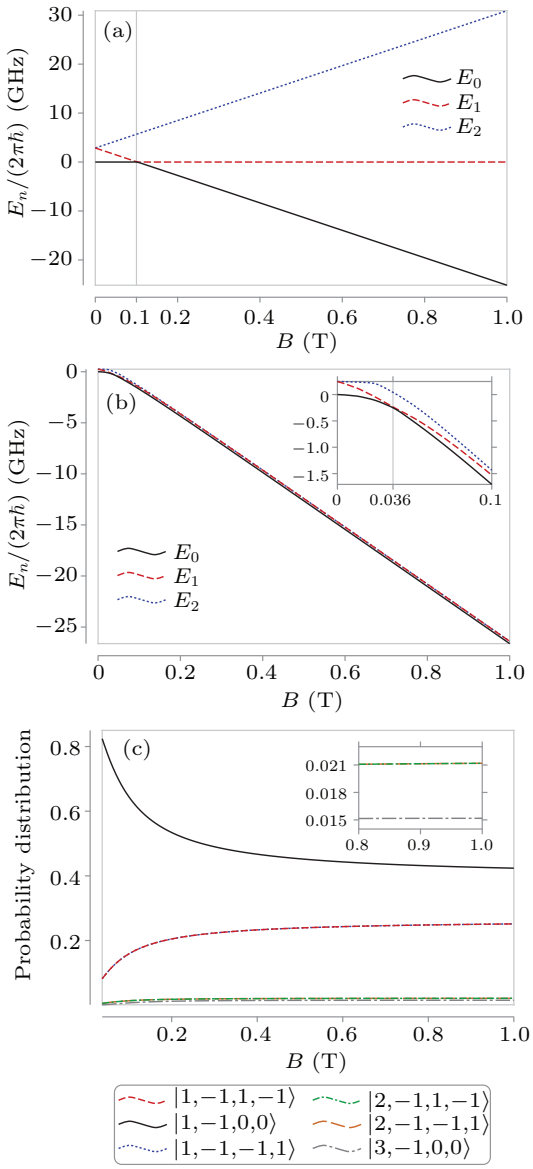


Fig. 3. (a) The energy levels of the spin Hamiltonian changing with the external magnetic field B. The crossing of the lowest two energy levels is at $B_0 \approx 0.1$ T. (b) The energy levels of the full spin-rotation Hamiltonian in Eq. (1) with $J_{\max} = 4$. The crossing is at $B_0 \approx 0.036$ T. (c) The main probability distribution of the ground state on base kets $|Jm_Jk_Jk_K\rangle$ with $J_{\max} = 4$. The insets of (b) and (c) show more details by zooming in.

From Figs. 3(a) and 3(b), we observe that in the same magnetic field, the energies of the ground state for our system are similar to those of the Hamiltonian without considering the rotation given by Eq. (41). However, our ground states become highly entangled states which mainly involve six components as shown in Fig. 3(c). We can see that $k_K = \pm 1$ gives $k_J = \mp 1$ and $k_K = 0$ gives $k_J = 0$. As the magnetic field strength increases, the entanglement increases and the probability of $k_K = \pm 1$ increases while the probability of $k_K = 0$ decreases. The spin component state of the ground state can be used to reflect the total angular moment state and the entanglement between them.

4. Entanglement of thermal equilibrium state

When our quantum system interacts with its thermal environment, it will finally arrive at a steady state: the thermal equilibrium state. Now we are ready to study the entanglement properties in these thermal equilibrium states, which will be useful to guide us to provide a natural protocol to prepare entanglement between nanodiamond rotation and NV^- center spin.

4.1. Entanglement of ground states

First we study the entanglement properties of the ground state, i.e., the thermal equilibrium state when the temperature approaches to zero. For a ground state $|G(B)\rangle_{JS}$ in magnetic field B, the entanglement entropy is defined as

$$S(\rho_S(B)) = -\operatorname{Tr}_S \rho_S(B) \log_2(\rho_S(B)), \tag{42}$$

where $\rho_S(B)$ is the reduced spin density matrix of $|G(B)\rangle_{JS}$. Because the dimension of the Hilbert space of NV^- center spin $d_S = 3$, the entanglement entropy $S(\rho_S) \leq \log_2 3$, where the equality is taken if and only if the ground state $|G(B)\rangle_{JS}$ is maximally entangled.

Numerical results on the entanglement entropy $S(\rho(B))$ are shown in Fig. 4(a). With the increase of magnetic field B, the entanglement of the ground state grows from 0 to approximately $\log_2 3$, which implies that the ground state approaches to a highly entangled state in a large magnetic field B. It seems that there is a curve peak of Ψ_1 at $B_0 \approx 0.036$ T in Fig. 4(a). This is due to the crossing of the lowest two energy levels (see the inset in Fig. 3(b)), which also causes the similar phenomena shown in Fig. 5. And we notice that the excited state has non-vanishing entanglement at $B = 0$ in Fig. 4(a), which causes the non-vanishing negativity for $B = 0$ only at finite temperatures because the thermal equilibrium state is a mixture of all eigenstates. As for why there is entanglement at $B = 0$, it comes from the coupled terms like $\hat{J}_i'\hat{K}_i'$ in Eq. (6) which usually represent the Barnett and Einstein–de Haas effect.[29–31]

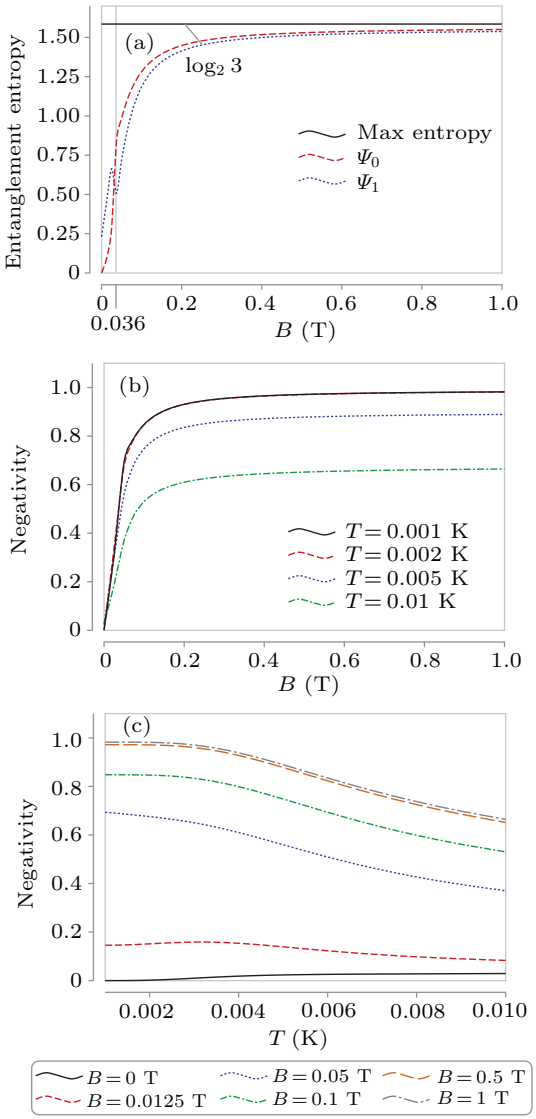


Fig. 4. The size of the particle $a = 1$ nm. (a) The entanglement entropy of the ground state and the first excited state compared with the maximum entanglement entropy for the maximum angular quantum number $J_{\max} = 4$. The negativity of the thermal entanglement state changing (b) with magnetic field B at some fixed temperatures T and (c) with absolute temperature at some fixed magnetic fields B.

4.2. Entanglement of thermal equilibrium states at low temperatures

At temperature T, the thermal equilibrium state can be represented as

$$\rho_{JS}(B,T) = \frac{1}{Z}\sum_i \mathrm{e}^{-\beta E_i}|\Psi_i\rangle\langle\Psi_i|, \tag{43}$$

where the partition function $Z = \sum_i \mathrm{e}^{-\beta E_i}$, and $|\Psi_i\rangle$ is the eigenvector of H with eigenvalue E_i, which has been obtained numerically in the previous section.

Because the thermal equilibrium state $\rho_{JS}(B,T)$ is a mixed state, its entanglement can not be characterized by the entanglement entropy $S(\rho_S)$, which is valid for characterization of entanglement for pure states. To study the entanglement property of the thermal equilibrium state, we introduce another entanglement measure, negativity,[32,33]

$$\mathcal{N}(\rho_{JS}) = \sum_{\lambda<0} |\lambda| = \frac{||\rho_{JS}^{T_S}||_1 - 1}{2}, \tag{44}$$

where $\rho_{JS}^{T_S}$ is the partial transpose of spin index for the bipartite mixed state ρ_{JS}, and λ is the eigenvalue of $\rho_{JS}^{T_S}$. The negativity corresponds to the absolute value of the sum of negative eigenvalues of $\rho_{JS}^{T_S}$. $||\rho_{JS}^{T_S}||_1$ is the trace norm of $\rho_{JS}^{T_A}$. The negativity $\mathcal{N}$ is a computable measure of entanglement for a mixed state and vanishes for separable states.

The numerical results of the negativity are shown in Fig. 4(b). It is observed in Fig. 4 that for a given temperature T, the negativity increases asymptotically to a maximum value with increasing magnetic field B. The lower the temperature, the larger the maximal value of the negativity. As shown in Fig. 4(c), for a fixed magnetic field B, the negativity decreases with increasing absolute temperature T. The larger the magnetic field, the larger the negativity. Our numerical results show that to obtain a thermal equilibrium state highly entangled, we need to increase the magnetic field above 0.5 T and decrease the temperature below 2 mK.

Based on the above numerical results, we propose a simple protocol to asymptotically prepare a highly entangled state between mechanical rotation of the nanodiamond and the electron spin of NV^- center. First, cool down the system to below 2 mK at zero or weak external magnetic field strength. Then adiabatically boost the magnetic field strength to above $B = 0.5$ T and keep the system still at low enough temperature. Finally in thermal equilibrium, we get the thermal equilibrium state highly entangled.

5. Discussion and conclusion

The degree of entanglement is different in different frames. A direct calculation shows that the complete set of commuting observables should be $\{\hat{\boldsymbol{L}}^2, \hat{L}_3, \hat{L}'_3, \hat{\boldsymbol{S}}^2, \hat{S}_3\}$ in space-fixed frame $\{\boldsymbol{e}_1, \boldsymbol{e}_2, \boldsymbol{e}_3\}$, and the Hamiltonian is

$$\begin{aligned} H =& \hbar D\left(\sum_{i=1}^{3}\hat{S}_i\boldsymbol{e}_i\cdot\boldsymbol{e}'_3\right)^2 + \frac{\hbar^2\hat{\boldsymbol{L}}^2}{2I_1} \\ &+ \frac{\hbar^2(I_1-I_3)\hat{L}'^2_3}{2I_1I_3} + g\mu_{\mathrm{B}}B\hat{S}_3. \end{aligned} \tag{45}$$

One can solve this eigen problem following the same procedure in this paper. When our model is solved in the space-fixed frame, the entanglement of the ground state and the first excited state is shown in Fig. 5, which is qualitatively different from that in Fig. 4(a). It is the global transformation between the two sets of bases that induces the entanglement variation. The difference in entanglement for the same states comes from the fact that the degrees of freedom being entangled we consider are different in the two sets of bases. This is consistent with physical interpretation that in the space-fixed frame

strong enough magnetic field makes the spin mainly occupying $|1,-1\rangle$ in the low energy states. Then from the view point in space-fixed frame, boosting magnetic field strength just results in opposite effect, disentanglement, compared with the view in the body-fixed frame.

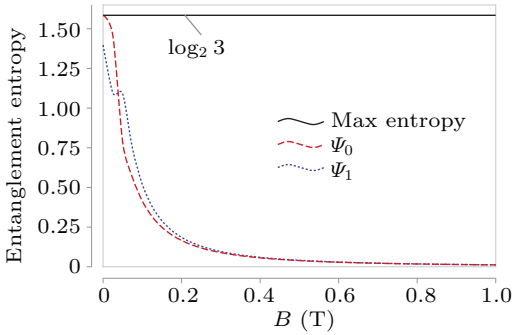


Fig. 5. The entanglement entropy of the ground state and the first excited state solved in the space-fixed frame with cutoff $L_{\max} = 4$.

We propose a theoretical model to describe a rotating nanodiamond with an embedded NV$^-$ center manipulated by a static external magnetic field. While, there are still many challenges that need to overcome to bring the primary theoretical model to practical experiment. For example, the nanodiamonds with NV$^-$ are usually charged and would gain magnetic moment through rotating. The inertia moments of such small nanodiamond are not easy to determine. Factors such as gravity, noise of the environment, the trap potential and so on need to be studied in more practical situation. And the detection of entanglement is usually very tough such as tomography of the state and entanglement witness. While, indirect detection by reading the spin state and scanning the energy levels employing optically detected magnetic resonance and single-photon detector may give some possible ways to examine the entanglement information of this system. Indeed, the practical problems which are not considered in this paper need to be further studied.

In our protocol to prepare entanglement, we propose to adiabatically boost the magnetic field strength. Theoretically, however, we do not require the boosting to be adiabatic, a sudden change of the magnetic field strength may also work after a much longer equilibrium time.

In conclusion, we explore the entanglement properties of a rotating nanodiamond with an embedded NV$^-$ center in an external magnetic field in a thermal equilibrium state, which includes the ground state as a special case. We find that the degree of entanglement depends on the degrees of freedom chosen in the two frames. The entanglement between nanodiamond rotation and NV$^-$ center spin can be controlled by an external magnetic field and the temperature: larger magnetic field strength and lower temperature result in more entanglement between the rotation and the spin. Our numerical results show that in our system setting when the magnetic field strength is tuned above 0.5 T and the temperature is controlled below 2 mK, the thermal equilibrium state will be an almost maximally entangled state. Thus we propose a theoretical protocol to realize the highly entangled states of the spin–rotation coupled system asymptotically. The entanglement between the spin (a microscopic degree) and the rotation (a mesoscopic degree) is not only of usefulness in quantum coherent control of two or multi quantum degrees of freedom, but also of interest in fundamental problems of quantum mechanics such as detection and utilization of quantum rotation of nanoparticles to explore the border between quantum world and classical world.[34]

Appendix A: D-matrix and Euler rotations

In this appendix, we give some details of the D-matrix of Euler rotations. We have chosen $\{\boldsymbol{e}_1,\boldsymbol{e}_2,\boldsymbol{e}_3\}$ to represent the space-fixed frame and $\{\boldsymbol{e}'_1,\boldsymbol{e}'_2,\boldsymbol{e}'_3\}$ the body-fixed frame. In the view of passive rotations, we consider $\boldsymbol{e}'_i$ is rotated to $\boldsymbol{e}_i$ by rotation operator $\hat{R}$, i.e., $\boldsymbol{e}_i = \hat{R}\boldsymbol{e}'_i = \sum_{j=1}^3 R_{ji}\boldsymbol{e}'_j$, where $R_{ji} \equiv \boldsymbol{e}'_j \cdot \boldsymbol{e}_i$. While in the view of active rotations, we usually define the rotation operator as $\boldsymbol{e}'_i = \hat{Q}\boldsymbol{e}_i$ which maps a vector $\boldsymbol{e}_i$ to a new vector $\boldsymbol{e}'_i$ in the same frame. It is clear to see that $\hat{R} = \hat{Q}^{-1}$ which usually gives the inverse relation of passive and active views of the same rotation transformation. In our paper, we choose the passive view on account of the two coordinate frames. We choose Euler angles $\{\alpha,\beta,\gamma\}$ to represent the rotation from space-fixed frame $\{\boldsymbol{e}_1,\boldsymbol{e}_2,\boldsymbol{e}_3\}$ to body-fixed frame $\{\boldsymbol{e}'_1,\boldsymbol{e}'_2,\boldsymbol{e}'_3\}$, which are shown in Fig. 2.

According to quantum mechanics, the generator of $\hat{R}$ is angular momentum $\hbar\hat{\boldsymbol{L}}$, especially in the space-fixed frame, $[\hat{L}_i,\hat{L}_j] = \mathrm{i}\sum_k \varepsilon_{ijk}\hat{L}_k$, where $i,j,k \in \{1,2,3\}$ with $\hat{L}_i \equiv \boldsymbol{e}_i \cdot \hat{\boldsymbol{L}}$ and ε_{ijk} is an antisymmetric tensor with $\varepsilon_{123} = 1$. Let $\hat{D}$ be the representation of the rotation operator $\hat{R}$ in Hilbert space, we have

$$\hat{D}(\alpha,\beta,\gamma) = \exp(\mathrm{i}\gamma\hat{L}_3)\exp(\mathrm{i}\beta\hat{L}_2)\exp(\mathrm{i}\alpha\hat{L}_3). \tag{A1}$$

And the space base kets relations are defined as $\hat{D}^\dagger(\alpha,\beta,\gamma)|\{\boldsymbol{e}'_i\}\rangle = |\{\hat{R}\boldsymbol{e}'_i\}\rangle = |\{\boldsymbol{e}_i\}\rangle$. In particular, for any vector operator $\hat{\boldsymbol{A}}$, $\hat{D}^\dagger\hat{\boldsymbol{A}}\hat{D} = \hat{Q}^{-1}\hat{\boldsymbol{A}} = \hat{R}\hat{\boldsymbol{A}}$. Then $\hat{D}^\dagger\hat{A}_i\hat{D} = \boldsymbol{e}_i \cdot \hat{D}^\dagger\hat{\boldsymbol{A}}\hat{D} = \boldsymbol{e}_i \cdot \hat{R}\hat{\boldsymbol{A}} = \hat{A}'_i$. Since in the space-fixed frame, $\hat{\boldsymbol{e}}'_l$ is a vector operator, $[\hat{L}_i, \hat{\boldsymbol{e}}'_l \cdot \boldsymbol{e}_j] = \mathrm{i}\sum_k \varepsilon_{ijk}\hat{\boldsymbol{e}}'_l \cdot \boldsymbol{e}_k$. More importantly, with the definition $\hat{L}'_i \equiv \hat{\boldsymbol{e}}'_i \cdot \hat{\boldsymbol{L}} = \sum_{j=1}^3 \hat{\boldsymbol{e}}'_i \cdot \boldsymbol{e}_j\hat{L}_j$, we have the following relations: $[\hat{L}_i,\hat{L}'_j] = 0$, $[\hat{L}'_i,\hat{L}'_j] = -\mathrm{i}\sum_k \varepsilon_{ijk}\hat{L}'_k$. Given the eigenstates $|LMK\rangle$ of $\{\hat{\boldsymbol{L}}^2,\hat{L}_3,\hat{L}'_3\}$, the eigenfunctions are

$$\begin{aligned}
&\langle\{\boldsymbol{e}_i\}|LMK\rangle = \langle\{\hat{R}\boldsymbol{e}'_i\}|LMK\rangle = \langle\{\boldsymbol{e}'_i\}|\hat{D}|LMK\rangle \\
&= \sum_{M'K'} \langle\{\boldsymbol{e}'_i\}|LM'K'\rangle\langle LM'K'|\hat{D}|LMK\rangle &\text{(A2)}\\
&= \sum_{M'} \langle\{\boldsymbol{e}'_i\}|LM'K\rangle\langle LM'K|\hat{D}|LMK\rangle &\text{(A3)}\\
&= \sum_{M'} \langle\{\boldsymbol{e}'_i\}|LM'K\rangle\langle LM'K|\hat{D}|LMK\rangle\delta_{M'K} &\text{(A4)}\\
&= \langle\{\boldsymbol{e}'_i\}|LKK\rangle\langle LK|\hat{D}|LM\rangle. &\text{(A5)}
\end{aligned}$$

From Eq. (A2) to Eq. (A3), we have used the communication relations of $\hat{L}_i$ and $\hat{L}'_i$, and in Eq. (A5) we omit the same K index. The Eq. (A4) is valid because

$$\begin{aligned}&\langle LM'K|\hat{L}_3\hat{D}|LMK\rangle = M'\langle LM'K|\hat{D}|LMK\rangle\\&= \langle LM'K|\hat{D}\hat{D}^\dagger\hat{L}_3\hat{D}|LMK\rangle = \langle LM'K|\hat{D}\hat{L}'_3|LMK\rangle\\&= K\langle LM'K|\hat{D}|LMK\rangle, \qquad \text{(A6)}\\&\text{i.e.,}\quad \langle LM'K|\hat{D}|LMK\rangle = \langle LM'K|\hat{D}|LMK\rangle\delta_{M'K}. \qquad \text{(A7)}\end{aligned}$$

When the rotations are described by the Euler angles, $\langle LK|\hat{D}|LM\rangle = D^{(L)}_{KM}(\alpha,\beta,\gamma)$, and Eq. (A5) gives us the eigenfunction Eq. (29).

Appendix B: Convergence tests

In this appendix, we display the convergence tests of the cutoff of maximum angular momentum $J_{\max}$ in our numerical calculation.

Fidelity is a measure of the "closeness" of two quantum states and is defined as $F(\rho,\sigma) = \left(\mathrm{tr}\sqrt{\sqrt{\rho}\sigma\sqrt{\rho}}\right)^2$. In the special case where ρ and σ are pure quantum sates, namely, $\rho = |\psi_\rho\rangle\langle\psi_\rho|$ and $\sigma = |\psi_\sigma\rangle\langle\psi_\sigma|$, the definition reduces to the squared overlap between the states: $F(\rho,\sigma) = |\langle\psi_\rho|\psi_\sigma\rangle|^2$. We check the fidelity between the ground states in Fig. B1(a) (the 1st excited states in Fig. B1(b)) of $J_{\max} = 4$ and $J_{\max} \in \{5,6,7,8\}$, and see that fidelity of larger cutoff ($J_{\max} \geq 4$) changes very little.

As a comparison with Fig. 4(a) which has cutoff $J_{\max} = 4$, a cutoff of $J_{\max} = 8$ is shown in Fig. B1(c). For the thermal equilibrium states, we check their negativity with several cutoff $J_{\max} \in \{2,3,4,5,6\}$ at temperature $T = 10$ mK which is shown in Fig. B1(d). It is clear to see that the negativity is convergent for $J_{\max} \geq 4$.

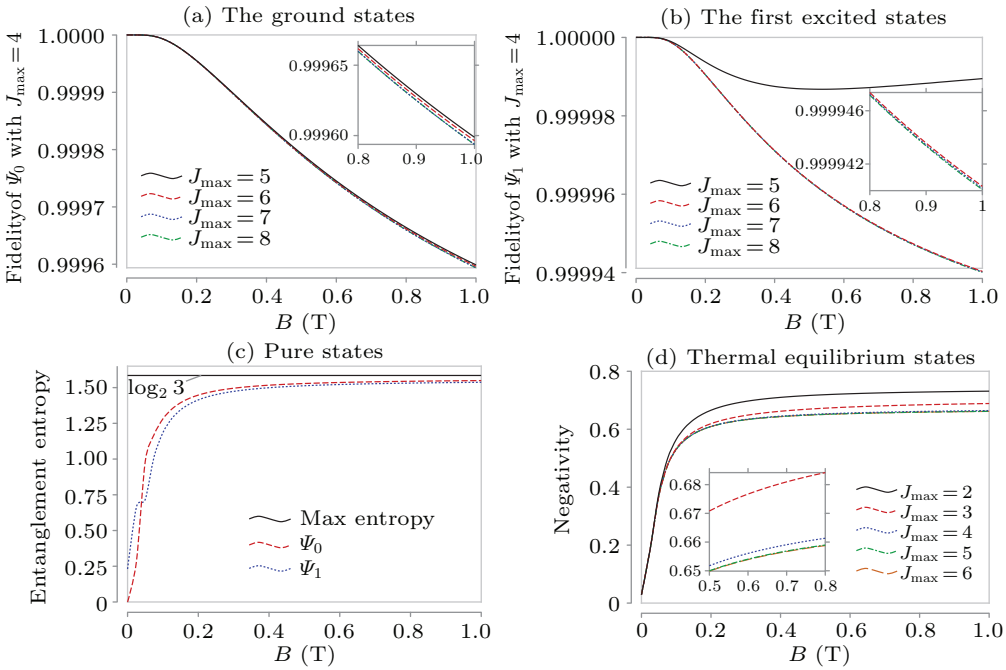


Fig. B1. The fidelity between the (a) ground states ((b) 1-st excited states) of $J_{\max} = 4$ and $J_{\max} \in \{5,6,7,8\}$. (c) The entanglement entropy with cutoff $J_{\max} = 8$. (d) The negativity of the thermal equilibrium states with different cutoff $J_{\max} \in \{2,3,4,5,6\}$ at temperature $T = 10$ mK.

Acknowledgements

Project supported by the National Key Research and Development Program of China (Grant Nos. 2021YFA0718302 and 2021YFA1402104), the National Natural Science Foundation of China (Grant No. 12075310), and the Strategic Priority Research Program of Chinese Academy of Sciences (Grant No. XDB28000000).

References

[1] Doherty M W, Manson N B, Delaney P, Jelezko F, Wrachtrup J and Hollenberg L C L 2013 *Phys. Rep.* **528** 1
[2] Chu Y and Lukin M D 2017 *Quantum Optics and Nanophotonics* (1st edn.) (Oxford University PressOxford) pp. 229–270
[3] Awschalom D D, Hanson R, Wrachtrup J and Zhou B B 2018 *Nat. Photonics* **12** 516
[4] Gieseler J, Deutsch B, Quidant R and Novotny L 2012 *Phys. Rev. Lett.* **109** 103603
[5] Delić U, Reisenbauer M, Dare K, Grass D, Vuletić V, Kiesel N and Aspelmeyer M 2020 *Science* **367** 892
[6] Tebbenjohanns F, Mattana M L, Rossi M, Frimmer M and Novotny L 2021 *Nature* **595** 378
[7] Yin Z Q, Li T, Zhang X and Duan L M 2013 *Phys. Rev. A* **88** 033614
[8] Yin Z, Zhao N and Li T 2015 *Science China Physics, Mechanics & Astronomy* **58** 1
[9] Wan C, Scala M, Morley G W, Rahman A A, Ulbricht H, Bateman J, Barker P F, Bose S and Kim M S 2016 *Phys. Rev. Lett.* **117** 143003
[10] Pedernales J S, Morley G W and Plenio M B 2020 *Phys. Rev. Lett.* **125** 023602
[11] Arita Y, Mazilu M and Dholakia K 2013 *Nat. Commun.* **4** 2374
[12] Hoang T M, Ma Y, Ahn J, Bang J, Robicheaux F, Yin Z Q and Li T 2016 *Phys. Rev. Lett.* **117** 123604
[13] Kuhn S, Kosloff A, Stickler B A, Patolsky F, Hornberger K, Arndt M and Millen J 2017 *Optica* **4** 356
[14] Kuhn S, Stickler B A, Kosloff A, Patolsky F, Hornberger K, Arndt M and Millen J 2017 *Nat. Commun.* **8** 1670

[15] Rashid M, Toroš M, Setter A and Ulbricht H 2018 *Phys. Rev. Lett.* **121** 253601
[16] Delord T, Nicolas L, Chassagneux Y and Hétet G 2017 *Phys. Rev. A* **96** 063810
[17] Delord T, Huillery P, Nicolas L and Hétet G 2020 *Nature* **580** 56
[18] Stickler B A, Papendell B, Kuhn S, Schrinski B, Millen J, Arndt M and Hornberger K2018 *New J. Phys.* **20** 122001
[19] Stickler B A, Hornberger K and Kim M S 2021 *Nature Reviews Physics* **3** 589
[20] Perdriat M, Huillery P, Pellet-Mary C and Hétet G 2022 *Phys. Rev. Lett.* **128** 117203
[21] Rusconi C C, Perdriat M, Hétet G, Romero-Isart O and Stickler B A 2022 *Phys. Rev. Lett.* **129** 093605
[22] Chitambar E and Gour G 2019 *Rev. Mod. Phys.* **91** 025001
[23] Biedenharn L C and Louck J D 1981 *Angular Momentum in Quantum Physics: Theory and Application* number v. 8 in Encyclopedia of Mathematics and Its Applications; Section, Mathematics of Physics (Reading, Mass: Addison-Wesley Pub. Co., Advanced Book Program)
[24] Landau L D and Lifshitz E M 2013 *Quantum Mechanics: Non-Relativistic Theory* (Vol. 3) (Elsevier)
[25] Yamanouchi K 2012 *Quantum Mechanics of Molecular Structures* (Berlin, Heidelberg: Springer Berlin Heidelberg)
[26] Loubser J H N and van Wyk J A 1978 *Rep. Prog. Phys.* **41** 1201
[27] Rusconi C C and Romero-Isart O 2016 *Phys. Rev. B* **93** 054427
[28] Hudak B M and Stroud R M 2023 *ACS Nano* **17** 7241
[29] Einstein A 1915 *Naturwissenschaften* **3** 237
[30] Richardson O W 1908 *Physical Review (Series I)* **26** 248
[31] Barnett S J 1915 *Phys. Rev.* **6** 239
[32] Vidal G and Werner R F 2002 *Phys. Rev. A* **65** 032314
[33] Horodecki R, Horodecki P, Horodecki M and Horodecki K 2009 *Rev. Mod. Phys.* **81** 865
[34] Aspelmeyer M, Kippenberg T J and Marquardt F 2014 *Rev. Mod. Phys.* **86** 1391